New $Na_{1+x}Ge_2(SiO_4)_x(PO_4)_{3-x}$ NASICON Series with Improved Grain and Grain Boundary Conductivities

Jairo F. Ortiz-Mosquera, Adriana M. Nieto-Muñoz,* and Ana C. M. Rodrigues

ACCESS | Metrics & More | Article Recommendations

ABSTRACT: In this study, we synthesize glass-ceramics of the new $Na_{1+x}Ge_2(SiO_4)_x(PO_4)_{3-x}$ NASICON (Na super-ionic conductor) series to evaluate the effect of Si^{4+}/P^{5+} substitution on the structural, microstructural, and electrical properties of the $NaGe_2(PO_4)_3$ system. From X-ray diffraction, the presence of the NASICON phase is confirmed in all glass-ceramics. An expansion of the unit cell volume suggesting an increase in the bottleneck of the NASICON structure is also observed. Impedance spectroscopy allowed the separation of grain and grain boundary contributions. We observe that the grain conductivity is higher than the specific grain boundary conductivity in all of the investigated compositions ($0 \leq x \leq 0.8$). The Si^{4+}/P^{5+} substitution causes an enhancement of about 2 and 3 orders of magnitude in the grain and specific grain boundary conductivities, respectively. This behavior is attributable to the introduction of new charge carriers (Na^+) in the NASICON structure and a decrease in the activation energy. Finally, the lowest activation energy for grain (0.586 eV) is observed in the $x = 0.6$ sample, which indicates the easiest displacement of ions in the investigated series, suggesting that this composition presents the most suitable bottleneck size for (Na^+) sodium ion conduction.

KEYWORDS: glass-ceramics, NASICON structure, grain, grain boundary conductivity, brick-layer model, bottleneck
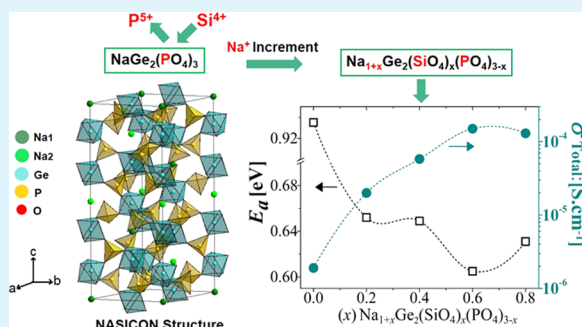
1. INTRODUCTION

NASICON-type materials (Na super-ionic conductor) are known for their high ionic conductivity with values between 10^{-4} and 10^{-1} S·cm^{-1} at 300 °C in the case of Na^+ ionic conductors, favored by their three-dimensional structure displaying interconnected conduction channels in which sodium (Na^+) ions can move easily with a low activation energy for ionic conductivity.[1−4] The general molecular formula of these materials may be represented by $Na_{1+2w+x-y+z}M(II)_wM(III)_xM(V)_yM(IV)_{2-w-x-y}(SiO_4)_z$-$(PO_4)_{3-z}$, where M is a pentavalent, tetravalent, or trivalent cation such as Nb^{5+}, Ti^{4+}, Ge^{4+}, Sn^{4+}, Sc^{3+}, or Hf^{3+}.[1] The NASICON compounds can be synthesized in a wide range of compositions since their structure accepts iso- and aliovalent substitutions in the position of the M ion.[5,6] Moreover, P^{5+} can be substituted by Si^{4+}.[4,7−9] All of these aliovalent substitutions are performed to increase the number of charge carriers by balancing the total charge of the compound and, therefore, also improve the ionic conductivity. Thus, the sodium-ion-conducting NASICON series in which the P^{5+} ions are replaced by Si^{4+}, such as $Na_{1+x}Zr_2P_{3-x}Si_xO_{12}$ (2.0 × 10^{-1} S·cm^{-1} at 300 °C), $Na_{1+x}Hf_2P_{3-x}Si_xO_{12}$ (1.7 × 10^{-1} S·cm^{-1} at 250°), and $Na_{3+x}Sc_3Si_xP_{3-x}O_{12}$ (6.9 × 10^{-4} S·cm^{-1} at 25 °C), stand out because they exhibit significantly high ionic conductivities.[4,8,9]

Among the possible synthesis processes of NASICON compounds, the glass-ceramic route, which consists of the controlled crystallization of a precursor glass, presents the advantage of allowing the microstructure control of the samples by applying different crystallization heat treatments to the parent glass. Thus, materials with low porosity and thus optimized electrical properties may be obtained.[5−7] An interesting system for synthesizing NASICON glass-ceramics is $NaGe_2(PO_4)_3$ (NGP) since its precursor glass ($Na_2O-GeO_2-P_2O_5$) exhibits two glass-former oxides in its composition, GeO_2, and P_2O_5. The NASICON crystalline structure obtained after crystallization heat treatment is rhombohedral and consists of PO_4 tetrahedra linked to the GeO_6 octahedra[6,10] (see Figure 1a). In this structure, there are two interstitial sites for Na^+ ions (Na1 and Na2) that are coordinated by six oxygens within an antiprism (Figure 1b). Sodium ions move from a Na1 to a Na2 site through the bottleneck, which is formed by two oxygen triangles that share
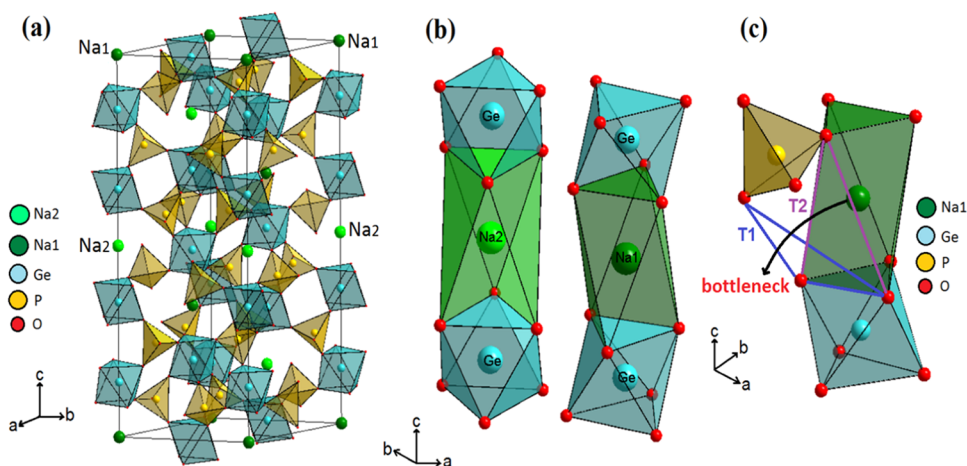
Figure 1. (a) Unit cell of the $NaGe_2(PO_4)_3$ NASICON-type structure; (b) octahedral coordination of Na1 and Na2 sites; and (c) bottleneck representation.

the edge of a GeO_6 octahedron and that are also separated by a PO_4 tetrahedron (Figure 1c).

In our previous work,[6] we obtained glass-ceramics from the NGP system by replacing the Ge^{4+} ions by Al^{3+}, thus forming the $Na_{1+x}Al_xGe_{2-x}(PO_4)_3$ (NAGP) series. An increase in the total ionic conductivity of 2 orders of magnitude (from 10^{-6} to 10^{-4} $S \cdot cm^{-1}$, at 300 °C) was evidenced due to the inclusion of aluminum and a consequent increase in the sodium ion concentration. Different Ge^{4+} substitutions by aliovalent ions (Ga^{3+} and Y^{3+}) in the NGP compound have also been reported.[11] However, it is noteworthy that the substitution of the P^{5+} ion, to the best of our knowledge, was never performed in the $NaGe_2(PO_4)_3$ system. Therefore, to evaluate the effect of the Si^{4+}/P^{5+} substitution on the ionic conductivity of the NGP system, we synthesized the glass-ceramics of the new $Na_{1+x}Ge_2(SiO_4)_x(PO_4)_{3-x}$ (NGSP) series. Electrical conductivity was measured by impedance spectroscopy, which allowed the separation of grain and grain boundary contributions. A comprehensive analysis of grain boundary conductivity was performed by calculating the specific grain boundary conductivity using the brick-layer model (BLM). In addition, we presented a detailed discussion about the correlation between the structural, microstructural, and electrical properties of this new NASICON series.

2. EXPERIMENTAL PROCEDURES

2.1. Glass and Glass-Ceramic Synthesis. The $Na_{1+x}Ge_2(SiO_4)_x(PO_4)_{3-x}$ (NGSP) ($0 \leq x \leq 1.0$) precursor glasses were synthesized by melting adequate quantities of reagent-grade chemicals such as Na_2CO_3 (Vetec, 99.5%), GeO_2 (Aldrich, 99.9%), SiO_2 (Zetasil, 99%), and $(NH_4)_2HPO_4$ (Aldrich, 98%). The nominal composition of glasses is listed in Table 1. Initially, the powders were weighed and mixed using a rotary jar mill for 12 h. Subsequently, the mixed powders were placed in a platinum crucible and heated up to 700 °C for 1 h in a tubular electrical furnace to release the ammonia (NH_3), carbon dioxide (CO_2), and water (H_2O) from the starting reagents. Finally, batches of 20 g were melted at 1250−1280 °C for 30 min, and the resultant melt was poured and splat-cooled between two steel plates. The transparent glasses were annealed at a temperature 40 °C lower than the T_g (glass transition temperature) for 2 h to release the thermal stresses and then cooled down slowly to room temperature.

To obtain the glass-ceramic samples, the precursor glasses were crystallized for 3 h at their respective crystallization temperatures (T_x), which was determined from thermal characterization by

Table 1. Nominal Composition (mol %) and Characteristic Temperatures, T_g (Glass Transition Temperature) and T_x (Onset of Crystallization Peak), of $Na_{1+x}Ge_2(SiO_4)_x(PO_4)_{3-x}$ Parent Glasses

x	Na_2O	GeO_2 [mol %]	SiO_2	P_2O_5	T_g [K] [±2 K]	T_x [K] [±2 K]
0.0	13.0	50.0	0.0	38.0	884	939
0.2	14.0	48.0	5.0	33.0	850	917
0.4	16.0	45.0	9.0	30.0	816	905
0.6	17.0	43.0	13.0	26.0	791	896
0.8	19.0	42.0	17.0	23.0	783	919
1.0^a	20.0	40.0	20.0	20.0	752	a

^{a}For the $x = 1.0$ glassy sample, the crystallization peak was not observed.

differential scanning calorimetry (DSC). The crystallized samples exhibited an opaque white appearance.

2.2. Glass and Glass-Ceramic Characterization. Glassy samples were analyzed by differential scanning calorimetry (DSC-Netzsch 404) to find out the glass transition (T_g) and crystallization (T_x) temperatures. The measurements were performed using a platinum crucible in the temperature range from 30 to 1000 °C with a heating rate of 10 °C·min⁻¹ in an air atmosphere.

Powder X-ray diffraction (XRD) patterns were recorded at room temperature using a Rigaku Ultima IV X-ray diffractometer to confirm the amorphous nature of glasses and to identify the crystalline phases of glass-ceramic samples. The XRD patterns were collected between 10 and 80° with a 0.02° step size and 0.6 s counting time with the Cu Kα radiation generated at 20 mA and 40 kV. The powder patterns were indexed using Crystallographica Search-Match software,[12] and Rietveld refinement was carried out with Topas-Academic (version 6)[13] using the Inorganic Crystal Structure Database (ICSD).[14]

The experimental density values of the NGSP precursor glasses (ρ_{glass}) and single-phase glass-ceramics (ρ_{gc}) were obtained by Archimedes' principle, using a Mettler-Toledo AX-204 analytical lab balance and water as the fluid. The ρ_{glass} and ρ_{gc} values were calculated from the average of seven measurements performed for each composition, which also allowed us to calculate the standard deviation.

The microstructure of the $Na_{1+x}Ge_2(SiO_4)_x(PO_4)_{3-x}$ ($0 \leq x \leq 0.8$) glass-ceramics was observed by means of a scanning electron microscope (SEM-Phillips XL30 FEG) on fractured surfaces.

The ionic conductivities of NGSP glass-ceramics were determined by impedance spectroscopy using a NOVOCONTROL Alpha-A high-performance frequency analyzer in the 1 MHz−100 mHz frequency range with a voltage amplitude of 300 mV. Measurements were

performed from 50 to 300 °C with a BDS-1200 sample holder inserted into a NOVOTHERM furnace, which allows a temperature precision of ± 0.1 °C. Before the impedance tests, samples with a thickness and surface of around 2 mm and 25 mm^2, respectively, were metalized with gold on both parallel sides using the QUORUM Q150R ES equipment.

3. RESULTS AND DISCUSSION

3.1. DSC Analysis. From the DSC thermograms of the different $Na_{1+x}Ge_2(SiO_4)_x(PO_4)_{3-x}$ parent glasses, two thermal events were identified. The first one is an inflection of the baseline in the endothermic direction and corresponds to the glass transition temperature (T_g), while the second is an exothermic peak and indicates the crystallization of the glasses. The crystallization temperature (T_x) is obtained at the onset of the crystallization peak. Figure 2a shows the DSC curve for x = 0.4 as an example, and Table 1 summarizes the characteristic temperatures of all synthesized parent glasses.
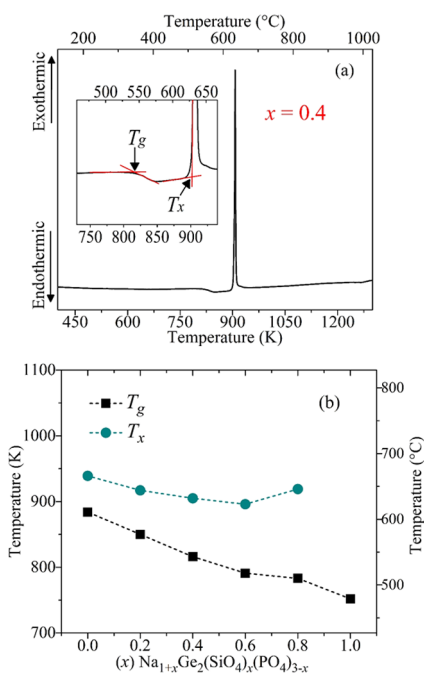

Figure 2. (a) DSC thermogram of $Na_{1+x}Ge_2(SiO_4)_x(PO_4)_{3-x}$ (x = 0.4) parent glass at a heating rate of 10 K·min^{-1}, indicating the glass transition temperature, T_g, and the crystallization temperature, T_x. (b) Characteristic temperatures (T_g and T_x) as a function of the silicon content (x) in $Na_{1+x}Ge_2(SiO_4)_x(PO_4)_{3-x}$ (NGSP) parent glasses. The dashed lines serve as a guide for the eye in (b).

The DSC thermogram in Figure 2a shows a sharp crystallization peak, which indicates an easy crystallization of the glass. Moreover, high stability against crystallization was observed for the x = 1.0 glass, since an exothermic peak for this composition was not observed. For this reason, glass ceramics were not attempted to be obtained from the glass with this composition.

Figure 2b shows a decrease of T_g as silicon (Si^{4+}) and sodium (Na^+) ions are introduced in the $Na_{1+x}Ge_2(SiO_4)_x(PO_4)_{3-x}$ system while the crystallization temperature T_x does not exhibit significant variations. This behavior of T_g has already been observed in our previous study carried out on NASICON precursor glasses containing silicon,[7] and the decrease in T_g was attributed to the depolymerization

of the phosphate chain and the consequent increase in the number of nonbridging oxygen, promoted by the addition of Na_2O, which is a modifier oxide for the glassy structures. On the other hand, the slight increase of T_x in x = 0.8 indicates that the effect of SiO_2 is more significant on the glass network for higher percentages of silicon, that is, the thermal energy needed to crystallize the glassy samples should be increased. In fact, this behavior is in good agreement with the absence of T_x in sample with x = 1.0.

3.2. X-ray Diffraction. X-ray diffraction patterns (Figure 3) confirmed the amorphous nature of
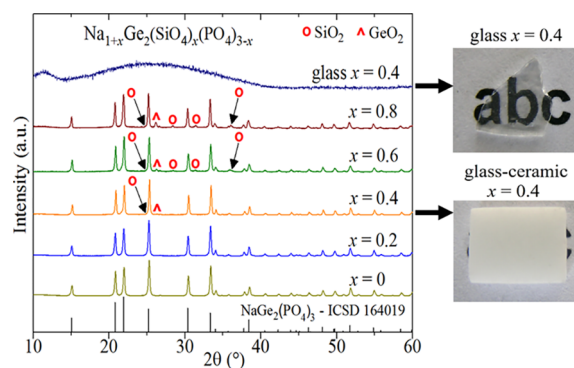

Figure 3. X-ray diffraction pattern of the parent glass for x = 0.4 and of $Na_{1+x}Ge_2(SiO_4)_x(PO_4)_{3-x}$ glass-ceramics. The black lines below the patterns show the peak locations for the $NaGe_2(PO_4)_3$ NASICON-type structure (space group $R\overline{3}$ ICSD file card no. 164019). Thus, all peaks not attributed to SiO_2 or GeO_2 belong to the $NaGe_2(PO_4)_3$ phase.

$Na_{1+x}Ge_2(SiO_4)_x(PO_4)_{3-x}$ parent glasses and their successful crystallization after heat treatment performed at their respective T_x for 3 h. XRD patterns also show the formation of the $NaGe_2(PO_4)_3$ NASICON-type structure (space group $R\overline{3}$ ICSD file card no. 164019) as the majority phase in all investigated glass-ceramics.

Table 2 summarizes the percentages of the crystalline phases observed in $Na_{1+x}Ge_2(SiO_4)_x(PO_4)_{3-x}$ glass-ceramics, the lattice constants of the NASICON structure, the theoretical density (ρ_t) derived from Rietveld refinements, and the experimental density values for glasses (ρ_{glass}) and glass-ceramics (ρ_{gc}) determined by Archimedes' principle.

Table 2 shows, as expected, that the densities of precursor glasses are lower than those of the corresponding glass-ceramics. Indeed, due to the open nature of the glass network, glass crystallization generally leads to more dense materials. It is also observed that the glass-ceramics of x = 0.0 and 0.2 compositions exhibited high experimental density values, which correspond to 97.4 and 97.9% of the theoretical density, respectively. These results show that the glass-ceramic route is a suitable method to synthesize materials with dense microstructures. A high relative density is a desirable characteristic in polycrystalline materials since it favors ionic conductivity, which allows a better performance as solid electrolytes in batteries.[15−17] On the other hand, due to the presence of secondary phases, density measurements were not performed for samples with $x \geq 0.4$ (Figure 3).

Figure 4a illustrates the percentage of crystalline phases quantified from Rietveld refinement, and Figure 4b shows the evolution of lattice parameters as a function of the silicon content (x) in $Na_{1+x}Ge_2(SiO_4)_x(PO_4)_{3-x}$ glass-ceramics.

Table 2. Lattice Constants ($a = b$, c), Unit Cell Volumes of the NASICON Structure, Percentage (wt %) of Crystalline Phases, Theoretical Densities (ρ_t), Experimental Densities of Precursor Glasses (ρ_g) and Glass-Ceramics (ρ_{gc}), Relative Density of Glass-Ceramics (ρ_r), and Agreement Factor R_{wp} Estimated by a Rietveld Analysis for $Na_{1+x}Ge_2(SiO_4)_x(PO_4)_{3-x}$ Glass-Ceramics[a]

a [Å]	c [Å]	V [Å³]	NASICON [wt %]	SiO₂ [wt %]	GeO₂ [wt %]	ρ_{glass} [g·cm⁻³]	ρ_t [g·cm⁻³]	ρ_{gc} [g·cm⁻³]	ρ_r[b] [%]	R_{wp}[c] [%]
8.1020(2)	21.5201(5)	1223.38(6)	100.0	0	0	3.397(1)	3.691(1)	3.594(1)	97.4	6.6
8.1050(1)	21.4960(4)	1224.00(5)	100.0	0	0	3.375(3)	3.659(2)	3.583(4)	97.9	7.0
8.1084(6)	21.5100(2)	1224.70(2)	98.0	1.8	0.2	3.248(2)				8.2
8.1114(6)	21.5060(2)	1225.40(2)	93.1	5.0	1.9	3.127(8)				8.6
8.1270(1)	21.5070(1)	1230.20(1)	87.6	9.4	3.0	3.087(4)				8.4

[a]The numbers within parentheses indicate mathematical errors given by the Rietveld refinement and for ρ_{glass} and ρ_{gc} indicate the standard deviation of seven measurements. [b]$\rho_r = (\rho_{gc}/\rho_t)(100)$. [c]$R_{wp} = \sum[w(y_o - y_c)^2/\sum wy_o^2]^{1/2}$; y_o = intensity of the X-ray pattern observed; y_c = intensity of the X-ray pattern calculated; $w = 1/y_o$.
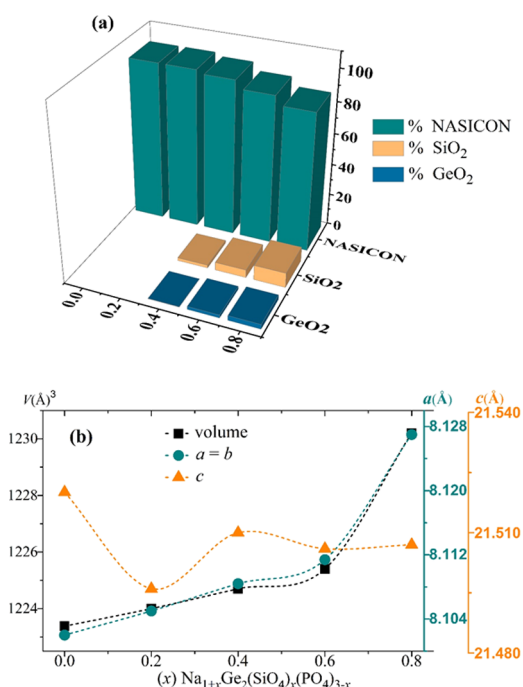

Figure 4. (a) Percentage of crystalline phases quantified by the Rietveld refinement and (b) variation of lattice constants and unit cell volumes of the NASICON structure, as a function of the silicon content (x) in the $Na_{1+x}Ge_2(SiO_4)_x(PO_4)_{3-x}$ glass-ceramics. The dashed lines in (b) are a guide for the eyes. Uncertainty values are smaller than the symbol size.

According to Table 2 and Figure 4a, a single-phase glass-ceramic was obtained with 100% of the desired NASICON phase for $x = 0.0$ and 0.2 compositions. For samples with $x \geq 0.4$, X-ray results show the formation of SiO_2 and GeO_2 in low quantities. Nieto-Muñoz et al.[7] suggest that the presence of secondary phases in glass-ceramics indicates the nonstoichiometry of parent glasses. However, it is important to mention that the NASICON phase is present in amounts greater than 87% in the whole range of compositions analyzed in this work.

On the other hand, the increase in the unit cell volume of the NASICON structure illustrated in Figure 4b is directly attributed to the increase in the lattice constant "a". Furthermore, the unit cell expansion is a consequence of the introduction of the larger Si^{4+} ion (0.26 Å) compared to P^{5+} (0.17 Å).[7,8,18,19] It is worth mentioning that for samples with $x \geq 0.4$, despite the presence of SiO_2 as a secondary phase, the volume of the NASICON structure keeps increasing. This behavior suggests that some part of the Si^{4+} ions are still being incorporated into the $NaGe_2(PO_4)_3$ phase, replacing P^{5+}. Since the size of the bottleneck is related to the unit cell volume of the NASICON structure,[1,2] it can be suggested that the inclusion of silicon in the NGSP system also increases the size of the bottleneck, through which sodium ions migrate. A similar behavior was reported in $Na_{1+y}Ti_2Si_yP_{3-y}O_{12}$ glass-ceramics for $x \leq 0.8$.[7]

Considering the solid solution limit of $Na_{1+x}Ge_2(SiO_4)_x(PO_4)_{3-x}$ system, one could argue that it could have been reached at $x = 0.2$ since secondary phases were observed in glass-ceramics for $x \geq 0.4$. However, the evolution of the unit cell volume of the NASICON structure may also suggest that the solid solution limit was not reached in the whole $0 \leq x \leq 0.8$ glass-ceramic range because its volume keeps increasing when silicon is added.

3.3. Microstructural Evolution. Figure 5 shows the SEM images of the fracture surface of $Na_{1+x}Ge_2(SiO_4)_x(PO_4)_{3-x}$ ($0 \leq x \leq 0.8$) glass-ceramics crystallized at their respective T_x for 3 h. The image sequences illustrate an increase in the average grain size as a function of the silicon content (x). It can be seen that crystallization heat treatment enabled us to obtain glass-ceramics with dense microstructures. The average grain size of spherical grains remains around 75 nm in the composition without silicon and approximately 77 nm in the sample with a lower silicon content ($x = 0.2$). Considering further silicon additions, the average grain size increases to the micrometer scale, reaching 0.2 and 1.2 μm for samples $x = 0.4$ and 0.6, respectively. Furthermore, the increase in the average grain size became more significant in the $x = 0.8$ sample ($\sim$22 μm) whose grains are 15 times larger compared to the average grain size of the $x = 0.6$ sample and approximately 290 times larger than that of the sample without silicon ($x = 0.0$). This notable increase in the average grain size is illustrated in the plot shown in Figure 5.

On the other hand, in samples for $x \geq 0.6$, some subgrains within the grains are observed (orange squares marked in the inset of $x = 0.6$ and 0.8 micrographs). EDS mapping of the $x = 0.6$ sample (not shown here) reveals a homogeneous distribution of Na, Ge, O, and P in the whole sample area, including the subgrains. Therefore, it may be suggested that these subgrains correspond to the NASICON phase. For $x = 0.8$, some spherical particles are observed within the grains (purple circles, inset in the micrograph). EDS mapping of this sample shows that these particles are rich in silicon (see Figure 5). Nieto-Muñoz et al.[7] also observed similar spherical particles in homologous glass-ceramics containing titanium instead of germanium. The authors confirmed that these particles appeared during the glass synthesis as a result of the tendency
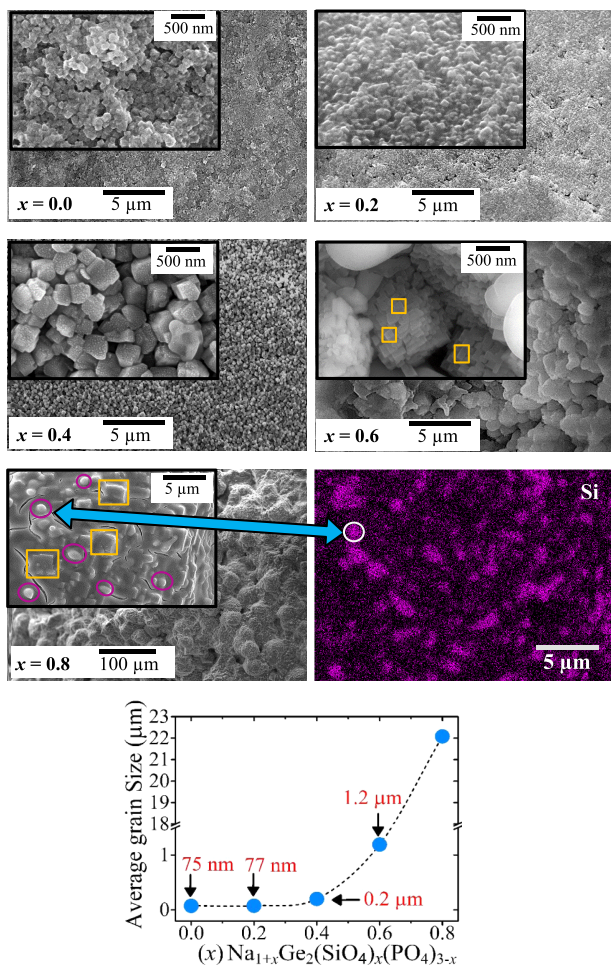
Figure 5. Scanning electron images of the fracture surface of $Na_{1+x}Ge_2(SiO_4)_x(PO_4)_{3-x}$ glass-ceramics, silicon EDS mapping of the sample for $x = 0.8$, and average grain size as a function of the silicon content in NGSP glass-ceramics. The purple circles at $x = 0.8$ represent the silicon-rich particles and the orange squares correspond to the subgrains in the micrographs for $x = 0.6$ and 0.8 samples. The dotted line is a guide for the eye, and uncertainty values are smaller than the symbol size in the plot.

for liquid−liquid phase separation in the parent glasses. Thus, it can be suggested that the silicon-rich particles observed in the mapping of the $x = 0.8$ sample correspond to vitreous silica. Additionally, the micrograph of this sample with a higher silicon content ($x = 0.8$) shows the presence of microcracks. The formation of microcracks is common in glass-ceramics since, during the crystallization process, tensile stresses are generated between the crystal and the glass matrix due to the difference between their thermal expansion coefficients.[20] This feature will be recalled in the discussion of the ionic conductivity results.

3.4. Ionic Conductivity Analysis. Figure 6 shows the complex impedance plots (Nyquist diagram) of $Na_{1+x}Ge_2(SiO_4)_x(PO_4)_{3-x}$ glass-ceramics at 230 °C for $x = 0.0$, 0.2, and 0.8 compositions. From the zoomed-in image at higher frequencies, it is evidenced that the total resistivity of the glass-ceramics with silicon ($x \geq 0.2$) is noticeably less than that for the silicon-free sample ($x = 0$). In the Nyquist plot of the $x = 0.0$ sample, the presence of two well-defined semicircles at high and low frequencies can be seen, which
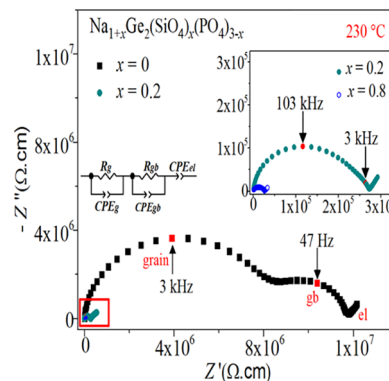

Figure 6. Complex impedance plots at 230 °C of $Na_{1+x}Ge_2(SiO_4)_x(PO_4)_{3-x}$ ($x = 0.0$, 0.2, and 0.8) glass-ceramics and the equivalent circuit used to fit the impedance data. The inset plot is a zoom-in of the higher-frequency region represented by the red square.

were associated with the grain and grain boundary electrical responses, respectively. The presence of two contributions is less evident for silicon-containing compositions, that is, $x \geq 0.2$ samples. In fact, as can be seen in the zoomed-in image in Figure 6, the grain boundary response for the $x = 0.2$ sample is evidenced by a distortion in the low-frequency region (around 3 kHz), indicating a strong overlap of grain and grain boundary contributions. The same distortion was observed in $0.4 \leq x \leq 0.8$ glass-ceramics. The straight line at lower frequencies in the complex impedance plots results from the blockage of sodium ions in the electrode and thus confirms the ionic nature of electrical conductivity in the NGSP samples.

The circuit used to fit the impedance data (see Figure 6) consists of two resistances (R_g and R_{gb} for grain and grain boundary, respectively), each of them in parallel to a constant phase element (CPE_i with $i = g$, gb), that is, $R_g \| CPE_g$ and $R_{gb} \| CPE_{gb}$. The constant phase elements were used to simulate the nonideal capacitance of the contributions in the grain and grain boundary, and each of these $R_i−CPE_i$ combinations was chosen to represent the electrical responses of the grain and grain boundary, respectively. The CPE_i has an associated impedance (Z_{CPE_i} with $i = g$, gb) according to[21]

$$Z_{CPE_i} = [Y_i(j\omega)^{n_i}]^{-1} \tag{1}$$

where ω is the angular frequency, and Y_i and n_i are values generated by the fitting procedure. The capacitance values associated with the grain (C_g) and grain boundary (C_{gb}) may be calculated using eq 2[21]

$$C_i = (R_i^{1-n_i/n_i})(Y_i^{1/n_i}) \tag{2}$$

where $i = g$, gb. The n_i term varies from 1 to 0 and indicates the degree of nonideal behavior of capacitance. When $n_i \to 1$, the constant phase element represents a purely capacitive process (ideal capacitance) and $Y_i \to C$. On the other hand, values of n_i lower than 1 mean a loss of the ideal behavior, that is, diffusion processes reduce the capacitance between electrodes.[9,21,22]

The C_g and C_{gb} capacitance values calculated from eq 2 are associated with the maximum of each semicircle in the Nyquist plot by the expression $\omega RC = 1$ ($\omega = 2\pi f$, where f is the relaxation frequency). As the temperature range analyzed varied for each sample (as will be noted in the Arrhenius plots), the impedance data at 150 °C for samples containing Si^{4+} ($x \geq 0.2$) and at 230 °C for the glass-ceramic with $x = 0.0$

Table 3. Fitting Data of Impedance Spectra of $Na_{1+x}Ge_2(SiO_4)_x(PO_4)_{3-x}$ Glass-Ceramics for x = 0.0 (230 °C)[a] and $x \geq 0.2$ (150 °C) and Grain Boundary Thickness (d) Calculated from eq 6

x	R_g [Ω]	Y_g [Ω^{-1} s^n]	n_g	C_g [F]	R_{gb} [Ω]	Y_{gb} [Ω^{-1} s^n]	n_{gb}	C_{gb} [F]	d [nm]
0.0[a]	7.5×10^6	7.4×10^{-12}	0.98	6.1×10^{-12}	4.2×10^6	9.0×10^{-10}	0.88	4.2×10^{-10}	1.09
0.2	2.4×10^6	5.7×10^{-12}	0.99	5.1×10^{-12}	1.7×10^6	5.7×10^{-10}	0.76	6.4×10^{-11}	7.03
0.4	3.3×10^5	9.8×10^{-12}	0.96	5.8×10^{-12}	4.5×10^5	8.4×10^{-9}	0.78	4.4×10^{-11}	25.90
0.6	2.4×10^5	1.3×10^{-11}	0.94	5.8×10^{-12}	1.0×10^5	2.3×10^{-9}	0.79	2.5×10^{-10}	33.82
0.8	1.1×10^5	1.2×10^{-11}	0.98	9.1×10^{-12}	2.7×10^5	1.2×10^{-10}	0.87	2.6×10^{-11}	504.01

[a]In the x = 0.0 sample, it was not possible to separately analyze the contributions of the grain and the grain boundary below 230 °C.

are summarized in Table 3. These C_g and C_{gb} values are in good agreement with the range proposed by Irvine et al.[23] for grain and grain boundary phenomena. The grain (R_g) and grain boundary (R_{gb}) resistances and the Y_i and n_i fitting parameters are also listed in Table 3.

The grain conductivity (σ_g), macroscopic grain boundary conductivity (σ_{ma-gb}), and total conductivity ($\sigma_{total-300\,°C}$) of $Na_{1+x}Ge_2(SiO_4)_x(PO_4)_{3-x}$ glass-ceramics were determined from the R_g and R_{gb} resistance values according to

$$\sigma_i = l/(R_i A) \tag{3}$$

where i = g, ma−gb, total. In eq 3, l is the sample thickness, A is the area of the electrode in contact with the sample, and R_g, R_{gb}, and R_{total} are the grain, grain boundary, and total resistances, respectively, estimated from the impedance data. The R_{total} was calculated from the sum of R_g and R_{gb}.

Considering that the volumetric fraction of the grain boundary is much smaller than the volumetric fraction of the grain, the macroscopic grain boundary conductivity (σ_{ma-gb}) was corrected by the inclusion in eq 3 of the grain boundary thickness (d) and the average grain size (D), giving access to the specific grain boundary conductivity σ_{sp-gb}, according to the brick-layer model[21,22,24]

$$\sigma_{sp-gb} = (l/R_{gb}A)(d/D) \tag{4}$$

From the combination of eqs 3 and 4, the relationship between macroscopic and specific grain boundary conductivities can be determined according to

$$\sigma_{ma-gb} = (\sigma_{sp-gb})(D/d) \tag{5}$$

On the other hand, assuming that the dielectric constant in the grain and grain boundary are the same ($\varepsilon_g = \varepsilon_{gb}$)[21,24,25]

$$d/D = C_g/C_{gb} \tag{6}$$

Thus, according to eqs 4 and 6

$$\sigma_{sp-gb} = (l/R_{gb}A)(C_g/C_{gb}) \tag{7}$$

Therefore, the specific grain boundary conductivity can be determined from the capacitances associated with the grain (C_g) and the grain boundary (C_{gb}), according to eq 7, or from the grain boundary thickness (d) and the average grain size (D), according to eq 4.

To understand the variation of the ionic conductivity in $Na_{1+x}Ge_2(SiO_4)_x(PO_4)_{3-x}$ glass-ceramics with temperature, we also calculated the activation energy (E_a) for ionic conduction and the pre-exponential factors (σ_0) from the Arrhenius equation

$$\sigma = \sigma_0 \exp(-E_a/k_B T) \tag{8}$$

where T and k_B are the absolute temperature and the Boltzmann constant, respectively. The σ_0 term is related to

parameters such as the carrier concentrations (n), the ionic charge (Ze), the hopping frequency (ν_0), and the jump distance (λ) according to[5]

$$\sigma_0 \approx n(Ze)^2\lambda^2\nu_0/kT \tag{9}$$

Figure 7 illustrates the Arrhenius plots of the grain, macroscopic grain boundary, specific grain boundary, and total conductivities of $Na_{1+x}Ge_2(SiO_4)_x(PO_4)_{3-x}$ glass-ceramics.

Table 4 summarizes the experimental values of the pre-exponential terms (log σ_{0i} with i = g, gb, and T), the activation energies of total (E_a), grain (E_{a-g}), and grain boundary (E_{a-gb}) contributions, and the grain (σ_g), total ($\sigma_{total-300°C}$), macroscopic (σ_{ma-gb}), and specific (σ_{sp-gb}) grain boundary conductivities at 300 °C. Activation energies and conductivity values were obtained from the linear regression of the experimental data in Figure 7, and these values are shown in Figure 8 as a function of the silicon content (x).

Table 4 shows that the parent glass for x = 0.2 exhibited higher activation energy and lower total ionic conductivity than the respective glass-ceramics. A similar behavior was observed in the other compositions. This result is explained by the formation of the three-dimensional NASICON phase after crystallization treatments, which favors the movement of ions and improves the ionic conductivity of a material. We have reported this typical behavior in sodium-ion-conducting glass-ceramics from other NASICON series.[5,6]

From Figure 8a, it is noted that the grain and specific grain boundary conductivities are improved as silicon is added to the $Na_{1+x}Ge_2(SiO_4)_x(PO_4)_{3-x}$ series. The increase in σ_g and σ_{sp-gb} is mainly explained by the decrease in the activation energy in each one of these regions when compared to the silicon-free sample (x = 0.0) (see Figure 8b). Some authors such as Losilla et al.,[2] Padma Kumar et al.,[26] and Taylor et al.[27] showed that the activation energy for the ionic conduction is related to the bottleneck size of the NASICON compounds. In their works, it was mentioned that there is an optimal size of bottlenecks for each NASICON series, in which the charge carrier ions move with the highest mobility and the lowest activation energy. Thus, the decrease in the activation energy observed in Figure 8b would be related to the increase in the volume of the unit cell or, in other words, to the expansion of the 3D bottleneck in the NASICON structure, as discussed in Section 3.2. It means that the increase in the bottleneck size produced by the replacement of P^{5+} by Si^{4+} would favor the movement of sodium ions in the grain and grain boundary. However, despite the continuous increase in the unit cell volume (Figure 4b) in the $Na_{1+x}Ge_2(SiO_4)_x(PO_4)_{3-x}$ series, an increase in the grain activation energy is noted for the x = 0.8 sample (see Figure 8b). A possible explanation for this increase is that the bottleneck size is too large at x = 0.8. In fact, as Taylor et al.[27] mentioned in their work, very small or very big bottlenecks
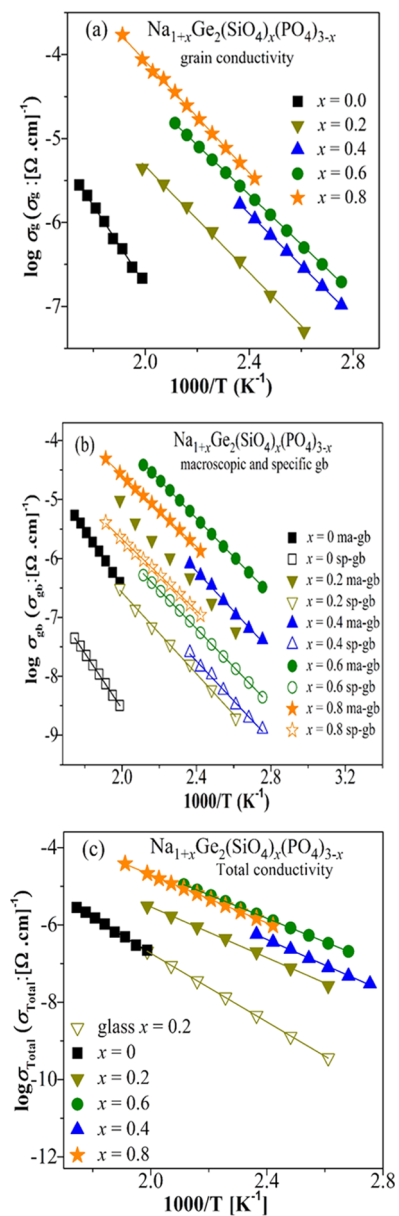
Figure 7. Arrhenius plot of (a) grain and (b) macroscopic and specific grain boundary electrical conductivities. (c) Arrhenius plot of the total electrical conductivity for $Na_{1+x}Ge_2(SiO_4)_x(PO_4)_{3-x}$ ($0.2 \leq x \leq 0.8$) glass-ceramics and for the $x = 0.2$ glass composition. Solid lines represent the linear regressions of the experimental data. Experimental uncertainties are smaller than the symbol sizes.

produce high activation energies. Thus, we observed in Figure 8b that the optimal bottleneck size for the ion diffusion is formed in the composition with $x = 0.6$ since the lowest grain activation energy (0.586 eV) is observed for this sample. In addition, from the EDS mapping performed in the sample for $x = 0.8$ (Figure 5), it can be suggested that the silicon-rich particles may disrupt the migration of Na^+ ions in the grain and consequently also increase the grain activation energy.

On the other hand, Figure 8b also shows a decrease in the activation energy of the grain boundary with the increase of x. If we assume that the SiO_2 and GeO_2 crystalline phases are segregated in the grain boundary, as usually occurs in polycrystalline materials,[28−30] the decrease in E_{a-gb} (even for samples with $x \geq 0.4$) suggests that these secondary phases do

not affect the conductivity in the intragranular region. Moreover, concerning the intragranular electrical behavior, we also evaluate the effect of the microstructure on the macroscopic grain boundary conductivity values, σ_{ma-gb} (see Table 4). Thus, we infer from eq 5 that larger grains ($>D$) favor the ionic conductivity in the grain−grain regions since the term D is directly proportional to σ_{ma-gb}.[31] In fact, from Table 4 and the plot in Figure 5, we observe that the σ_{ma-gb} ionic conductivity increases simultaneously as the P^{5+}/Si^{4+} replacement is performed and as the average grain size increases. However, for $x = 0.8$, a decrease in the macroscopic grain boundary conductivity is observed as compared to the σ_{ma-gb} for the $x = 0.6$ sample (see Table 4). The decrease in σ_{ma-gb} is possibly due to the presence of cracks (see Figure 5) that affect the contact area between grains.[32] This phenomenon is also reflected in the low value of $\log \sigma_{0-gb}$ for this sample, which is smaller than that for the other NGSP glass-ceramics (Table 4). In addition, we suggest that the significant increase in the grain boundary thickness (d) in the $x = 0.8$ sample (see Table 3) may also be responsible for the decrease in σ_{ma-gb} according to eq 5.

On the other hand, it is also observed (see Table 4 and Figure 8b) that the activation energy in the grain is lower than that of the grain boundary in all compositions of the NGSP series except in $x = 0.8$. Thus, the grain conductivity is higher than the specific grain boundary conductivity as expected (Figure 8a). Besides, if we exclude the $x = 0.0$ sample, a tendency of the pre-exponential factor of the grain ($\log \sigma_{0-gb}$) to increase is noted (Table 4). This behavior is expected since an increase in the density of Na^+ charge carrier ions is promoted by the Si^{4+}/P^{5+} substitution (see eq 9).

Finally, Figure 8c shows that adding silicon to the $NaGe_2(PO_4)_3$ sample decreased the activation energy from 0.935 eV ($x = 0.0$) to 0.605 eV ($x = 0.6$), and consequently, an improvement of approximately 2 orders of magnitude in the total ionic conductivity was reached.

4. SUMMARY AND CONCLUSIONS

In the present study, we successfully synthesized glass-ceramics of the new $Na_{1+x}Ge_2(SiO_4)_x(PO_4)_{3-x}$ ($0 \leq x \leq 0.8$) NASICON series. From X-ray diffraction in combination with Rietveld refinement, the NASICON phase was seen as the majority phase in all glass-ceramics (100 wt % for $x = 0.0$ and 0.2 and >87 wt % for $x \geq 0.4$). Besides, an expansion in the unit cell volume and, therefore, an increase in the bottleneck size were observed in the NASICON structure as a consequence of the introduction of the larger Si^{4+} ion (0.26 Å) compared to P^{5+} (0.17 Å).

By impedance spectroscopy, the improvement of grain (σ_g) (from 10^{-6} to 10^{-4} S·cm^{-1}) and grain boundary (σ_{gb}) electrical conductivities was confirmed. This increase was attributed to the increase in the Na^+ charge carrier concentration due to the P^{5+}/Si^{4+} substitution and the decrease in the activation energy.

The increase in the average grain size caused by silicon addition in the NGSP glass-ceramics also contributed to the enhancement of the macroscopic grain boundary conductivity (σ_{ma-gb}). The correction of the macroscopic grain boundary conductivity using BLM (brick-layer model) allowed us to evidence an increase of 3 orders of magnitude (10^{-8}−10^{-5} S·cm^{-1}) in the specific grain boundary conductivity (σ_{sp-gb}).

The grain conductivity (σ_g) was higher than the specific grain boundary conductivity (σ_{sp-gb}) in all compositions of the NGSP series since the activation energy in the grain (E_{a-g}) is

Table 4. Ionic Conductivities at 300 °C of the Grain (σ_g), Total ($\sigma_{total-300\,°C}$), Macroscopic (σ_{ma-gb}), and Specific (σ_{sp-gb}) Grain Boundary, Activation Energies of the Grain (E_{a-g}), Grain Boundary (E_{a-gb}), and Total (E_a) Conductivities, and Logarithm of the Pre-exponential Term of the Arrhenius Equation ($\log \sigma_{0i}$ with i = g, gb, and T) for Glass-Ceramics of the $Na_{1+x}Ge_2(SiO_4)_x(PO_4)_{3-x}$ ($0 \leq x \leq 0.8$) System and of the Parent Glass for $x = 0.2$[a]

sample	grain			grain boundary				total		
	E_{a-g} [eV]	$\log \sigma_{0-g}$ [σ_0: S·cm^{-1}]	σ_g [S·cm^{-1}]	E_{a-gb} [eV]	$\log \sigma_{0-gb}$ [σ_0: S·cm^{-1}]	σ_{ma-gb} [S·cm^{-1}]	σ_{sp-gb} [S·cm^{-1}]	E_a [eV]	$\log \sigma_{0-T}$ [σ_0: S·cm^{-1}]	$\sigma_{total-300\,°C}$ [S·cm^{-1}]
parent glass $x = 0.2$								0.868(3)	2.00(1)	2.3×10^{-6}
					glass-ceramics					
0	0.934(9)	2.68(9)	2.9×10^{-6}	0.937(7)	2.98(6)	5.6×10^{-6}	7.9×10^{-8}	0.935(9)	2.51(9)	1.9×10^{-6}
0.2	0.628(9)	1.01(8)	3.1×10^{-5}	0.688(9)	1.84(9)	6.2×10^{-5}	2.2×10^{-6}	0.652(9)	1.04(9)	2.0×10^{-5}
0.4	0.612(2)	1.51(3)	1.3×10^{-4}	0.670(9)	1.89(9)	1.1×10^{-4}	3.1×10^{-6}	0.649(8)	1.47(8)	5.8×10^{-5}
0.6	0.586(2)	1.42(1)	1.9×10^{-4}	0.646(3)	2.50(3)	6.6×10^{-4}	9.0×10^{-6}	0.605(1)	1.49(5)	1.5×10^{-4}
0.8	0.659(6)	2.57(6)	6.0×10^{-4}	0.602(4)	1.49(4)	1.6×10^{-4}	1.3×10^{-5}	0.631(3)	1.65(4)	1.3×10^{-4}

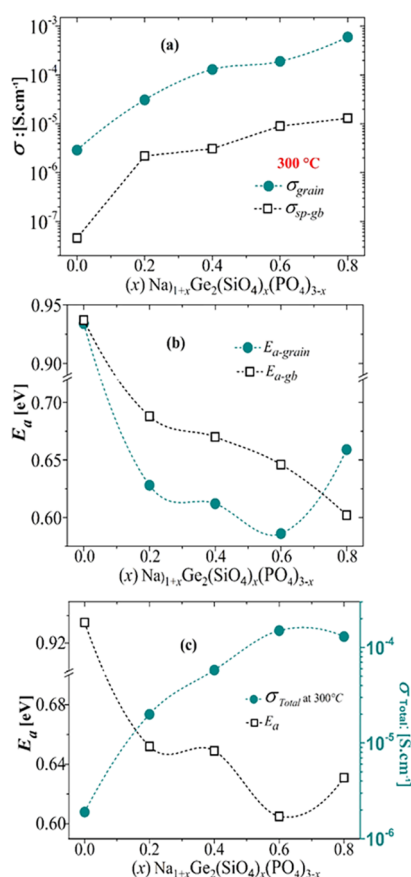[a]Numbers within parentheses represent the mathematical uncertainty.

Figure 8. (a) Grain and specific grain boundary conductivities, (b) activation energy of the grain and grain boundary, and (c) total conductivity at 300 °C and activation energy as a function of the silicon content in $Na_{1+x}Ge_2(SiO_4)_x(PO_4)_{3-x}$ glass-ceramics. The dashed lines are a guide for the eye, and uncertainty values are smaller than the symbol size.

always smaller than that of the grain boundary (E_{a-gb}). Therefore, as expected, the migration of ions is easier through the grains than through the grain boundaries.

Finally, the lowest grain (E_{a-g}) and total (E_a) activation energies were seen in the $x = 0.6$ composition, which indicates that the ideal bottleneck size for the displacement of Na^+ ions through the material was achieved in this composition.

AUTHOR INFORMATION

Corresponding Author

Adriana M. Nieto-Muñoz − *Programa de Pós-graduação em Ciência e Engenharia de Materiais, Universidade Federal de São Carlos, 13565-905 São Carlos, SP, Brazil;* orcid.org/0000-0002-6837-8988; Email: adriana.nieto@ppgcem.ufscar.br

Authors

Jairo F. Ortiz-Mosquera − *Programa de Pós-graduação em Ciência e Engenharia de Materiais, Universidade Federal de São Carlos, 13565-905 São Carlos, SP, Brazil;* orcid.org/0000-0001-9961-6769

Ana C. M. Rodrigues − *Departamento de Engenharia de Materiais, Universidade Federal de São Carlos, 13565-905 São Carlos, SP, Brazil;* orcid.org/0000-0003-1689-796X

Complete contact information is available at:
https://pubs.acs.org/10.1021/acsami.9b23065

Notes

The authors declare no competing financial interest.

REFERENCES

(1) Guin, M.; Tietz, F. Survey of the Transport Properties of Sodium Superionic Conductor Materials for Use in Sodium Batteries. *J. Power Sources* **2015**, *273*, 1056−1064.

(2) Losilla, E. R.; Aranda, M. A. G.; Bruque, S.; París, M. A.; Sanz, J.; West, A. R. Understanding Na Mobility in NASICON Materials: A Rietveld, ^{23}Na and ^{31}P MAS NMR, and Impedance Study. *Chem. Mater.* **1998**, *10*, 665−673.

(3) Anantharamulu, N.; Koteswara Rao, K.; Rambabu, G.; Vijaya Kumar, B.; Radha, V.; Vithal, M. A Wide-Ranging Review on Nasicon Type Materials. *J. Mater. Sci.* **2011**, *46*, 2821−2837.

(4) Goodenough, J. B.; Hong, H. Y.-P.; Kafalas, J. A. Fast Na^+-Ion Transport in Skeleton Structures. *Mater. Res. Bull.* **1976**, *11*, 203−220.

(5) Nieto-Muñoz, A. M.; Ortiz-Mosquera, J. F.; Rodrigues, A. C. M. The Role of Al^{+3} on the Microstructural and Electrical Properties of $Na_{1+x}Al_xTi_{2-x}(PO_4)_3$ NASICON Glass-Ceramics. *J. Alloys Compd.* **2020**, *820*, No. 153148.

(6) Ortiz-Mosquera, J. F.; Nieto-Muñoz, A. M.; Rodrigues, A. C. M. Precursor Glass Stability, Microstructure and Ionic Conductivity of Glass-Ceramics from the $Na_{1+x}Al_xGe_{2-x}(PO_4)_3$ NASICON Series. *J. Non-Cryst. Solids* **2019**, *513*, 36−43.

(7) Nieto-Muñoz, A. M.; Ortiz-Mosquera, J. F.; Rodrigues, A. C. M. Novel Sodium Superionic Conductor of the $Na_{1+y}Ti_2Si_yP3-yO_{12}$ Series for Application as Solid Electrolyte. *Electrochim. Acta* **2019**, *319*, 922−932.

(8) Vogel, E. M.; Cava, R. J.; Rietman, E. Na^+ Ion Conductivity and Crystallographic Cell Characterization in the Hf-Nasicon System $Na_{1+x}Hf_2Si_xP_{3-x}O_{12}$. *Solid State Ionics* **1984**, *14*, 1−6.

(9) Guin, M.; Tietz, F.; Guillon, O. New Promising NASICON Material as Solid Electrolyte for Sodium-Ion Batteries: Correlation between Composition, Crystal Structure and Ionic Conductivity of $Na_{3+x}Sc_2Si_xP_{3-x}O_{12}$. *Solid State Ionics* **2016**, *293*, 18−26.

(10) Zhao, D.; Xie, Z.; Hu, J.-M.; Zhang, H.; Zhang, W.; Yang, S.-L.; Cheng, W.-D. Structure Determination, Electronic and Optical Properties of $NaGe_2P_3O_{12}$ and $Cs_2GeP_4O_{13}$. *J. Mol. Struct.* **2009**, *922*, 127−134.

(11) Li, C.; Jiang, S.; Lv, J.-W.; Zheng, T. Ionic Conductivities of Na-Ge-P Glass Ceramics as Solid Electrolyte. *J. Alloys Compd.* **2015**, *633*, 246−249.

(12) Oxford Cryosystems. Crystallographica Search-Match. *J. Appl. Crystallogr.* **1999**, *32*, 379−380.

(13) Coelho, A. A.; Evans, J.; Evans, I.; Kern, A.; Parsons, S. The TOPAS Symbolic Computation System. *Powder Diffr.* **2011**, *26*, S22−S25.

(14) Belskly, A.; Hellendbrandt, M.; Karen, V. L.; Luksch, P. New Developments in the Inorganic Crystal Structure Database (ICSD): Accessibility in Support of Materials Research and Design. *Acta Crystallogr., Sect. B: Struct. Sci.* **2002**, *58*, 364−369.

(15) Famprikis, T.; Canepa, P.; Dawson, J. A.; Islam, M. S.; Masquelier, C. Fundamentals of Inorganic Solid-State Electrolytes for Batteries. *Nat. Mater.* **2019**, *18*, 1278−1291.

(16) Kim, Y.; Jo, H.; Allen, J. L.; Choe, H.; Wolfenstine, J.; Sakamoto, J. The Effect of Relative Density on the Mechanical Properties of Hot-Pressed Cubic $Li_7La_3Zr_2O_{12}$. *J. Am. Ceram. Soc.* **2016**, *99*, 1367−1374.

(17) Liu, Y.; Liu, J.; Sun, Q.; Wang, D.; Adair, K. R.; Liang, J.; Zhang, C.; Zhang, L.; Lu, S.; Huang, H.; Song, X.; Sun, X. Insight into the Microstructure and Ionic Conductivity of Cold Sintered NASICON Solid Electrolyte for Solid-State Batteries. *ACS Appl. Mater. Interfaces* **2019**, *11*, 27890−27896.

(18) Shannon, R. D. Revised Effective Ionic Radii and Systematic Studies of Interatomic Distances in Halides and Chalcogenides. *Acta Crystallogr., Sect. A* **1976**, *32*, 751−767.

(19) Fu, J. Fast Li^+ Ion Conduction in $Li_2O-Al_2O_3-TiO_2-SiO_2-P_2O_5$ Glass-Ceramics. *J. Am. Ceram. Soc.* **1997**, *80*, 1901−1903.

(20) Sakamoto, A.; Himei, Y.; Hashibe, Y. β-Spodumene Glass-Ceramic with Anomalous Low Thermal Expansion. *Adv. Mater. Res.* **2008**, *39−40*, 381−386.

(21) Barsoukov, E.; Macdonald, J. R. *Impedance Spectroscopy Theory, Experiment, and Applications*; John Wiley & Sons, 2005.

(22) Naqash, S.; Sebold, D.; Tietz, F.; Guillon, O. Microstructure-Conductivity Relationship of $Na_3Zr_2(SiO_4)_2(PO_4)$ Ceramics. *J. Am. Ceram. Soc.* **2019**, *102*, 1057−1070.

(23) Irvine, J. T. S.; Sinclair, D. C.; West, A. R. Electroceramics: Characterization by Impedance Spectroscopy. *Adv. Mater.* **1990**, *2*, 132−138.

(24) Chung, H.; Kang, B. Increase in Grain Boundary Ionic Conductivity of $Li_{1.5}Al_{0.5}Ge_{1.5}(PO_4)_3$ by Adding Excess Lithium. *Solid State Ionics* **2014**, *263*, 125−130.

(25) Haile, S. M.; Staneff, G.; Ryu, K. H. Non-Stoichiometry, Grain Boundary Transport and Chemical Stability of Proton Conducting Perovskites. *J. Mater. Sci.* **2001**, *36*, 1149−1160.

(26) Padma Kumar, P.; Yashonath, S. Ion Mobility and Levitation Effect: Anomalous Diffusion in Nasicon-Type Structure. *J. Phys. Chem. B* **2002**, *106*, 3443−3448.

(27) Taylor, B. E.; English, A. D.; Berzins, T. New Solid Ionic Conductors. *Mater. Res. Bull.* **1977**, *12*, 171−181.

(28) Samiee, M.; Radhakrishnan, B.; Rice, Z.; Deng, Z.; Meng, Y. S.; Ong, S. P.; Luo, J. Divalent-Doped $Na_3Zr_2Si_2PO_{12}$ Natrium Superionic Conductor: Improving the Ionic Conductivity via Simultaneously Optimizing the Phase and Chemistry of the Primary and Secondary Phases. *J. Power Sources* **2017**, *347*, 229−237.

(29) Verkerk, M. J.; Middelhuis, B. J.; Burggraaf, A. J. Effect of Grain Boundaries on the Conductivity of High-Purity $ZrO_2−Y_2O_3$ Ceramics. *Solid State Ionics* **1982**, *6*, 159−170.

(30) Verkerk, M. J.; Winnubst, A. J. A.; Burggraaf, A. J. Effect of Impurities on Sintering and Conductivity of Yttria-Stabilized Zirconia. *J. Mater. Sci.* **1982**, *17*, 3113−3122.

(31) Van Dijk, T.; Burggraaf, A. J. Grain Boundary Effects on Ionic Conductivity in Ceramic $Gd_xZr_{1-x}O_{2-(x/2)}$ Solid Solutions. *Phys. Status Solidi A* **1981**, *63*, 229−240.

(32) Mariappan, C. R.; Yada, C.; Rosciano, F.; Roling, B. Correlation between Micro-Structural Properties and Ionic Conductivity of $Li_{1.5}Al_{0.5}Ge_{1.5}(PO_4)_3$ Ceramics. *J. Power Sources* **2011**, *196*, 6456−6464.